Current flow in topological insulator Josephson junctions due to imperfections

Kiryl Piasotski [1,2,*] Omri Lesser [3,4] Adrian Reich [1] Pavel Ostrovsky [5] Eytan Grosfeld [6] Yuriy Makhlin [7,8] Yuval Oreg,[3] and Alexander Shnirman [1,2]

[1]*Institute for Theory of Condensed Matter (TKM), Karlsruhe Institute of Technology, 76131 Karlsruhe, Germany*
[2]*Institute for Quantum Materials and Technologies (IQMT), Karlsruhe Institute of Technology, 76021 Karlsruhe, Germany*
[3]*Department of Condensed Matter Physics, Weizmann Institute of Science, 7610001 Rehovot, Israel*
[4]*Department of Physics, Cornell University, Ithaca, New York 14853, USA*
[5]*Max Planck Institute for Solid State Research, 70569 Stuttgart, Germany*
[6]*Department of Physics, Ben-Gurion University of the Negev, Beer Sheva 84105, Israel*
[7]*Condensed-matter physics Laboratory, HSE University, 101000 Moscow, Russia*
[8]*Landau Institute for Theoretical Physics, 142432 Chernogolovka, Russia*

Recent experiments on planar superconductor-topological insulator-superconductor (S-TI-S) junctions, e.g., in the Corbino geometry, have reported low-temperature nonzero Josephson currents in states with integer fluxoid (flux) induced in the junction by a perpendicular magnetic field. This effect was discussed in connection with Majorana zero modes localized in Josephson vortices of such junctions. Here, we provide an explanation for this phenomenon, attributing it to imperfections. We focus on the "atomic" limit in which the low-energy bound states of different vortices do not overlap. In this limit, we can associate the nonvanishing critical current with the irregularities, e.g., in the junction's width. The low-temperature contribution to the current is provided by the bound states with low but nonzero energy. We also propose clear experimental tests based on microwave spectroscopy, revealing distinctive selection rules for vortex transitions.

I. INTRODUCTION

The Majorana zero modes in artificial topological superconductors [1] have been in focus of both academic and industrial research for the last two decades. The leading proposals allowing for experimental realization are the one-dimensional (1-D) semiconducting wires proximitized by regular superconductors [2,3], the extended planar (two-dimensional, 2-D) Josephson junctions on the surface of a three-dimensional (3-D) topological insulator [4,5] (Fu & Kane proposal) and the chains of magnetic adatoms on superconducting surfaces [6]. All these systems have by now been studied experimentally (see, e.g., Ref. [7] and many earlier works for 1-D wires, Ref. [8] for the planar Josephson junctions, and Ref. [9] for the chains of adatoms).

This paper is dedicated to the study of the planar (Fu & Kane) platform and is motivated by the recent spark in the associated experimental activity [8,10,11]. Whereas Ref. [8] addresses the Fraunhofer pattern in a long Josephson junction with open ends, in Refs. [10,11] long Josephson junctions of Corbino geometry were investigated. We focus here on the Corbino geometry because it allows us to avoid the compli-

cations related to the boundary conditions at the open ends. Indeed, in the Josephson junctions with the open ends one measures [8] the standard Fraunhofer pattern since arbitrary magnetic flux is allowed in the junction. The simplest approach of integrating the local current-phase relation over the length of the junction might be a good first approximation, but might also miss the subtle effects related to the boundary conditions at the open ends, i.e., the 1-D Majorana modes having to hybridize there with the continuum of modes. The Corbino geometry avoids all these complications but, on the other hand, is subject to flux (fluxoid) quantization. Thus one cannot measure the full Fraunhofer pattern but only the discrete points corresponding to the integer number of flux quanta, where naively the Josephson current should vanish.

We aim at elucidating the recently observed [10,11] nonvanishing Josephson currents in circular Corbino junctions when a nonzero number of flux quanta (fluxoids) are trapped in the ring. These should be closely related to the lifting of the zero nodes of the Fraunhofer pattern in the open-end junctions [8]. The fact that these Josephson currents emerge only at temperatures much lower than the superconducting gap, induced in the TI, leads us to believe that they are related to the low-energy Andreev states in the Josephson vortices (a.k.a. Caroli-de Gennes-Matricon, or CdGM, states [12]).

To explain this phenomenon we examine the atomic limit of the Josephson vortex lattice created by an external magnetic field in the TI part of the junction [13–16]. We observe that irregularities in, e.g., the width of the junction can explain the presence of the observed Josephson currents, as conjectured in Ref. [10]. Moreover, our simple estimates

---

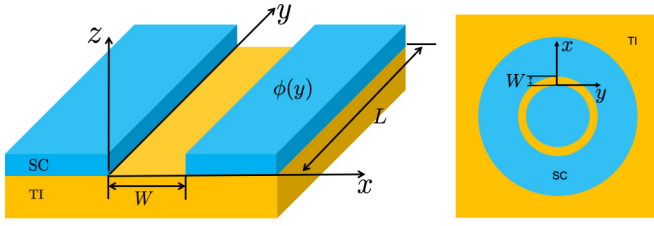*Contact author: kiryl.piasotski@kit.edu

FIG. 1. (left panel) Planar Josephson junction. (right panel) Corbino geometry Josephson junction.
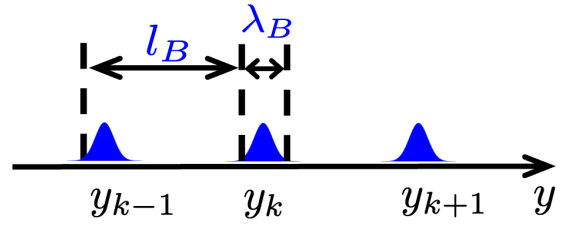

FIG. 2. A cartoon showing a chain of vortices at distance ℓ_B from each other. The low-energy CdGM states are localized at a distance $\lambda_B \ll \ell_B$.

reproduce correctly the magnitude of the current observed in the experiment [11].

We also study the current profiles associated with the individual CdGM states and show how these are modified by the imperfections. Finally, we investigate the microwave spectroscopy of the low-energy Andreev (CdGM) states. We predict very peculiar selection rules for the allowed transitions, characteristic for the Josephson vortices in long topological Josephson junctions.

II. THE SYSTEM

We start by describing a planar Josephson junction shown in Fig. 1 (left panel). Later we focus on the Corbino geometry and "transform" this into a ring shape, see Fig. 1 (right panel). To model this system we consider the following Hamiltonian [4,5,14,17]:

$$H = \frac{1}{2} \int dx \int_0^L dy \, \Psi^\dagger(\mathbf{r}) h \Psi(\mathbf{r}), \qquad (1)$$

where $\mathbf{r} \equiv (x, y)$, $h = \tau_z \{ v\boldsymbol{\sigma} \cdot [\mathbf{p} + e\mathbf{A}(\mathbf{r})\tau_z] - \mu(\mathbf{r}) \} + [\Delta(\mathbf{r})\tau_+ + \text{H.c.}]$ is the corresponding Bogoliubov–de Gennes Hamiltonian, and $\Psi(\mathbf{r}) = (\Psi_\uparrow(\mathbf{r}), \ \Psi_\downarrow(\mathbf{r}), \ \Psi_\downarrow^\dagger(\mathbf{r}), \ -\Psi_\uparrow^\dagger(\mathbf{r}))^T$ is the extended Nambu field. Here v is the bare Fermi velocity associated with the topological insulator's Dirac cone, $\mathbf{p} = -i\boldsymbol{\nabla} = -i(\partial_x, \ \partial_y)$ is the momentum operator, $\boldsymbol{\sigma} = (\sigma_x, \ \sigma_y)$ is the vector of Pauli matrices operating on the spin space, while the τ matrices are the set of Pauli matrices associated with the particle-hole basis.

The proximity-induced superconducting energy gap $\Delta(\mathbf{r})$ is assumed to have a step-like profile $\Delta(\mathbf{r}) = \Delta\Theta(-x) + e^{i\varphi(y)}\Delta\Theta(x - W)$, with the running phase $\varphi(y) = \frac{2\pi y}{\ell_B}$ arising from the external magnetic field treated in the Landau gauge [18]. Specifically, irrespectively of the nature of the screening of the magnetic field by the supercurrent (London or Pearl regimes), we argue that the following choice is always possible: $A_x(\mathbf{r}) = 0$, $A_y(\mathbf{r}) = A_y(x)$, and $\lim_{x \to -\infty} eA_y(x) = 0$, $\lim_{x \to \infty} eA_y(x) = -\frac{1}{2} \frac{d\varphi(y)}{dy} = -\frac{\pi}{\ell_B}$, i.e., A_y is there to compensate $\frac{d\varphi(y)}{dy}$ deep in the superconductor so that the supercurrent there vanishes (screening). For example, under the assumption of London screening, we obtain $\frac{d\varphi(y)}{dy} = \frac{2\pi}{\ell_B} = \frac{2\pi}{\Phi_0}(2\lambda_L + W)B$, where λ_L is the London's penetration depth.

To account for the renormalization of the chemical potential by the proximity to metallic superconductors, we follow Ref. [19] and consider a step-like profile of the chemical potential $\mu(\mathbf{r}) = \mu_S[\Theta(-x) + \Theta(x - W)] + \mu_N\Theta(x)\Theta(W - x)$, where, in the following, we assume μ_S to be the largest energy scale in our model (Andreev limit).

The low-lying excitations of the topological Josephson junction described by the Hamiltonian of Eq. (1) may be seen in certain regimes (to be specified below) as a quasi-one-dimensional lattice of Josephson vortex "atoms" [13–16]. Each of these atoms is centered around $y \approx y_k = k\ell_B + \ell_B/2$, such that $\phi(y_k) = (2k+1)\pi$. Each vortex hosts a number of localized orbitals (CdGM states). For the atomic limit to hold, the localization length of the low-energy orbitals λ_B (to be defined later) must be much smaller than the distance between the vortices ℓ_B, strongly suppressing the intervortex overlaps and, thus, rendering the vortex lattice into an array of nearly independent isolated atoms (see Fig. 2).

As we show in Appendix A that the kth atom is described by a two-component Nambu field $\psi_k(y)$ governed by the following effective 2×2 Dirac (Bogoliubov–de Gennes) Hamiltonian:

$$h_k^{\text{eff}} = \tfrac{1}{2}\{-i\partial_y, v_k(y)\}\rho_y + \varepsilon_k(y)\rho_z. \qquad (2)$$

In this Hamiltonian only the two lowest-energy bound states of the transverse part of the microscopic Hamiltonian (see Appendix A) are taken into account. In the limit $W < \xi \equiv v/\Delta$ considered in this paper these are the only in-gap states in the vicinity of the vortex center y_k. The new set of Pauli matrices ρ_x, ρ_y, ρ_z was introduced in order to avoid confusion with spin $\vec{\sigma}$ and Nambu $\vec{\tau}$ Pauli matrices of the microscopic Hamiltonian (1). Here $\varepsilon_k(y)$ solves the following transcendental equation (see Ref. [20]): $[\epsilon - i(\Delta^2 - \epsilon^2)^{1/2}]^2 = \Delta^2 e^{-2i\epsilon W/v} e^{i\varphi(y)}$, for y in the vicinity of y_k (see Fig. 2).

The y-dependent velocity $v_k(y)$, on the other hand, is deduced from the model parameters, including $\varepsilon_k(y)$, via the following formula (see Appendix A):

$$v_k(y) = \frac{v}{1 + \frac{W\tilde{\Delta}_k(y)}{v}} \left\{ \frac{\tilde{\Delta}_k(y)}{\mu_N} \sin\left(\frac{\mu_N W}{v}\right) + \frac{\tilde{\Delta}_k(y)}{\mu_S^2 + \tilde{\Delta}_k^2(y)} \left[\tilde{\Delta}_k(y) \cos\left(\frac{\mu_N W}{v}\right) - \mu_S \sin\left(\frac{\mu_N W}{v}\right) \right] \right\}, \qquad (3)$$

where $\tilde{\Delta}_k(y) \equiv [\Delta^2 - \varepsilon_k^2(y)]^{1/2}$ determines the localization of the vortex states in the x direction via $\approx e^{-\tilde{\Delta}_k(y)|x|/v}$.

Before proceeding any further, we find it instructive to discuss Eq. (3) in greater detail. First, considering the Andreev limit $\mu_S \gg \max\{\Delta,\ \mu_N,\ v/W\}$, we find

$$v_k \simeq \frac{v}{1 + \frac{W\tilde{\Delta}_k}{v}} \frac{\tilde{\Delta}_k}{\mu_N} \sin\left(\frac{\mu_N W}{v}\right), \qquad (4)$$

which at low energies $\tilde{\Delta}_k \simeq \Delta$ coincides with the result of Titov and Beenakker [19]. Note that in the limit $W \ll v/\mu_N$, Eq. (4) further simplifies to $v_k \simeq \tilde{\Delta}_k W$.

Considering another limiting case of equal chemical potentials $\mu_S = \mu_N = \mu$ at low energies $\tilde{\Delta}_k \simeq \Delta$, we recover the result of Fu and Kane [4].

In this manner, Eq. (3) serves to extend the previously established results. In the following sections, we operate within the physically relevant Andreev limit described by Eq. (4).

Now we proceed to study the spectrum of the Hamiltonian (2). First, we note that this Hamiltonian possesses charge conjugation $C = \rho_x K$ and chiral $S = \rho_x$ symmetries. It has a topologically protected zero-energy mode with the wave function given by

$$\chi_{k,0}(y) \propto \begin{pmatrix} 1 \\ \pm 1 \end{pmatrix} \frac{\exp\left(\mp \int^y dy' \frac{\varepsilon_k(y')}{v_k(y')}\right)}{\sqrt{v_k(y)}}, \qquad (5)$$

where the $\pm$ sign is chosen so that the resulting state is normalizable.

To get an idea about the excited states (cf. Refs. [13,14,16]), it is instructive to linearize $\epsilon_k(y)$ in the vicinity of $y = y_k$, i.e., $\epsilon_k(y) \approx \alpha_k(y - y_k)$ and fix the velocity as $v_k(y) \approx \bar{v}_k \equiv v_k(y_k)$. We obtain

$$h_k^{\text{eff}} \approx -i\bar{v}_k \rho_y \partial_y + \alpha_k(y - y_k)\rho_z. \qquad (6)$$

A simple estimate gives

$$\alpha_k \approx \frac{\Delta}{2} \frac{1}{1 + W/\xi} \frac{2\pi}{\ell_B}.$$

One observes [13,14,16] that the resulting Hamiltonian is that of the supersymmetric oscillator, and may be diagonalized exactly (see Appendix D). One finds that the excited states are exponentially localized in the Gaussian fashion

$$\propto \exp\left\{ -\frac{(y - y_k)^2}{2\lambda_{\text{B}k}^2} \right\},$$

with the localization length given by

$$\lambda_{\text{B}k} = \sqrt{\frac{\bar{v}_k}{\alpha_k}} \approx \left| \frac{v\ell_B \sin(\mu_N W/v)}{\pi \mu_N} \right|^{1/2}. \qquad (7)$$

The right-hand side (RHS) of this equation will depend on k if W or μ_N would become y dependent, as discussed below. We observe that the atomic limit $\lambda_B \ll \ell_B$ requires either $v/\mu_N \ll \ell_B$ and arbitrary W, or $W \ll \ell_B \ll v/\mu_N$. For definiteness we assume here the following experimentally relevant hierarchy of lengths: $W \ll \ell_B \sim \xi \ll v/\mu_N$. Then, $\bar{v}_k \sim \Delta W \sim vW/\xi \ll v$. Recall we assume the Andreev limit $\mu_S \gg \max\{\Delta,\ \mu_N,\ v/W\}$ leading to Eq. (4).

For the energy levels, one finds the following square root scaling $E_{n,k} = -E_{-n,k} = \omega_{\text{B}k}\sqrt{n}$, $n = 1, 2, 3 \ldots$, with the frequency given by

$$\omega_{\text{B}k} = \sqrt{2\bar{v}_k \alpha_k} = \frac{\Delta}{1 + W/\xi} \left| \frac{2\pi v \sin(\mu_N W/v)}{\mu_N \ell_B} \right|^{1/2}. \qquad (8)$$

Figure 3 shows the spectrum of a single Josephson vortex evaluated numerically by diagonalizing the Hamiltonian (2). In particular, Fig. 3(a) demonstrates the spectral flow of Andreev levels with the dimensionless magnetic field $2\pi\xi/\ell_B$, while Fig. 3(b) exemplifies that with the chemical potential in the junction region μ_N. As is apparent from Fig. 3, our low-energy formula (8) carefully captures both $2\pi\xi/\ell_B$ and μ_N dependencies of the spectrum.

We observe that irregularity could make the width $W(y)$ or the chemical potential $\mu_N(y)$ dependent on y. Then the eigenfrequencies $\omega_{\text{B}k}$ and the localization lengths $\lambda_{\text{B}k}$ would indeed depend on the location y_k of each vortex (cf. pinning) and would vary between vortices.

III. JOSEPHSON CURRENT DUE TO VARIATION OF THE WIDTH

We close the system into a ring of length $L = N\ell_B$ in the y direction. In the experiment, N and $\ell_B = L/N$ are determined by the external magnetic field, screening of the magnetic field (London or Pearl regimes), and the fluxoid quantization. The boundary conditions emerging upon encircling the ring are not important in the atomic limit [21]. This way we model the Corbino disk geometry junctions recently studied experimentally in Refs. [10,11].

We start by pointing out that, without irregularities, the total current in the system hosting an integer number $N = L/\ell_B \neq 0$ of flux quanta vanishes exactly because the externally induced phase difference φ_0, entering the problem via $\varphi(y) = 2\pi y/\ell_B + \varphi_0$, may be completely removed from consideration by the coordinate transformation $y \to y - \frac{\varphi_0}{2\pi}\ell_B$ (remember we are on a ring), thus rendering the Gibbs free energy independent of φ_0 and leading to the null Josephson current $J = \frac{2\pi}{\Phi_0}\partial_{\varphi_0}F = 0$. In contrast, if we allow any of the model parameters to have additional y dependence or introduce any y dependent perturbation, we cannot eliminate the
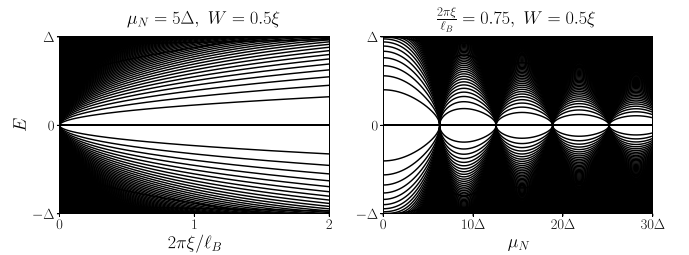

FIG. 3. Spectral flow of a single topological Josephson vortex. The left panel shows the evolution of the spectrum with dimensionless magnetic field $2\pi\xi/\ell_B \propto B$. The right panel shows the evolution of the vortex spectrum with the chemical potential of the central region, μ_N. Note that the spectrum condenses around the Fermi energy for the values of μ_N in resonance with the effective cavity modes $\mu_N = v\pi m/W$, $m \in \mathbb{Z}$.

external offset phase φ_0, which inevitably leads to the emergence of nonzero critical currents.

Perhaps, one of the simplest things to imagine is to assume that the width W admits for small variations along the junction $W = W(y)$. Another possibility are random gate charges leading to variations of $\mu_N(y)$.

Assuming such a variation to be slow on the scale of λ_{Bk}, we may roughly assume the frequency of the kth oscillator to change as

$$\omega_{B,k}(\varphi_0) \approx \frac{\Delta}{1 + W_k(\varphi_0)/\xi} \left| \frac{2\pi v \sin(\mu_N W_k(\varphi_0)/v)}{\mu_N \ell_B} \right|^{1/2}, \quad (9)$$

where $W_k(\varphi_0) = W(y_k + \frac{\varphi_0}{2\pi}\ell_B)$, giving rise to a nonzero current

$$I(\varphi_0) = -\frac{\pi}{\Phi_0} \sum_k \sum_{n=1}^{n_{\max}} \tanh\left(\frac{\beta E_{n,k}}{2}\right) \frac{\partial E_{n,k}}{\partial \varphi_0}. \quad (10)$$

In principle, $n_{\max}$ could be the number of energy levels that fit into the gap. This is a subtle issue because the continuum states over the gap could also contribute to the current. Here we focus on the contribution of the low-energy states only, $E_{n,k} \ll \Delta$, because these can be extracted by performing measurement at different temperatures.

Indeed, this simple consideration allows us to make a good connection with a recent experiment [11]. In that work, the critical current $I_c = \max_{\varphi_0 \in [0,2\pi)} I(\varphi_0)$ is measured at various temperatures. The experiment reveals that a drop in the temperature from $T = 1.6$ K to $T = 0.25$ K produces an increase in the $N \neq 0$ critical current from being roughly zero $I_c \approx 0$ to around $I_c \approx 10$ nA.

This result, when analyzed with the help of Eq. (10), immediately tells us that the observed effect was produced by the low-lying excitations of the system because it is their contribution that gets enhanced by the $\tanh(\beta E/2)$ function upon the temperature drop. Using the experimentally observed value of the zero-field ($N = 0$) critical current $I_c(B = 0) \approx 2$ μA (see Ref. [11]), as well as a rough estimate of the Corbino disk dimensions $L/W \approx 20$, we may recover the size of the energy gap from the approximate relation [19] $I_c(B = 0) \sim \frac{\pi\Delta}{\Phi_0}\frac{L}{W}$ to be $\pi\Delta/\Phi_0 \approx 100$ nA ($\Delta/k_B \approx 5$ K). For the contribution of the first CdGM state to the Josephson current at $T \ll E_{1,k} = \omega_{\mathrm{Bk}}$ we obtain

$$\delta I_1 = -\frac{\pi}{\Phi_0} \frac{\partial E_{1,k}}{\partial \varphi_0} \sim -\frac{\pi\Delta}{2\Phi_0} \sqrt{\frac{\ell_B}{2\pi W}} \frac{\partial W}{\partial y_k}. \quad (11)$$

Introducing a typical variation of the width δW and estimating roughly $|\partial W/\partial y_k| \sim \delta W/L = \delta W/(N\ell_B)$, we obtain

$$|\delta I_1| \sim \frac{\pi\Delta}{\Phi_0} \sqrt{\frac{W}{8\pi NL}} \frac{\delta W}{W} \sim 0.5 \text{ nA}/\sqrt{N}. \quad (12)$$

We have allowed for the width variations of the order of 10%, that is $\delta W/W \approx 0.1$. Taking into account that several

low-energy CdGM states can contribute and since $E_{n,k} = \sqrt{n}E_{1,k}$, i.e., $\delta I_n \sim \sqrt{n}\,\delta I_1$, we see that our simple logic gives rise to a correct quantitative estimate of the observed current [11]. An example of width irregularity is provided in Appendix B.

IV. CURRENT PROFILES OF INDIVIDUAL CDGM STATES

To elucidate how irregularities of the width W or the chemical potential μ_N generate Josephson current, we investigate here the contributions of the individual CdGM levels. We start again with the Hamiltonian of a single vortex (2). To derive the current-density operator, one can formally subject the system to an external flux $\varphi(y) \to \varphi(y) + 2\pi\Phi(t)/\Phi_0$ (see Refs. [22–24]), which, to the lowest order in perturbation theory, modifies the effective Hamiltonian (2) as

$$h_k^{\mathrm{eff}}(t) = -\frac{1}{2}\{v_k(y), p_y\}\rho_y + \varepsilon_k(y)\rho_z - j_k(y)\Phi(t), \quad (13)$$

where $j_k(y)$ is the projection of the current-density operator onto the low-energy subspace of the kth vortex and is given by (see Appendix C)

$$j_k(y) = \frac{\ell_B}{\Phi_0} \frac{\partial \varepsilon_k(y)}{\partial y} \rho_z. \quad (14)$$

Next, motivated by the approximate relation $v_k(y) \sim \Delta W(y)$, we linearize around $y = y_k$ and obtain $v_k(y) \approx \bar{v}_k + \gamma_k(y - y_k)$, where $\gamma_k = \Delta\partial W/\partial y|_{y=y_k}$. Assuming, as in (6), $\epsilon_k(y) = \alpha_k(y - y_k)$, we obtain

$$j_k(y) = (\ell_B \alpha_k/\Phi_0)\rho_z, \quad (15)$$

and

$$h_k^{\mathrm{eff}} = \frac{1}{2}\{-i\partial_y, v_k(y)\}\rho_y + \varepsilon_k(y)\rho_z$$

$$\approx -i\bar{v}_k\rho_y\partial_y + \alpha_k(y - y_k)\rho_z + \frac{\gamma_k}{2}\{-i\partial_y, (y - y_k)\}\rho_y. \quad (16)$$

We analyze (16) perturbatively (see Appendix D) and obtain two important conclusions: (a) The current profile of the zero (Majorana) level does not get any correction and remains zero, and (b) the current profile of the first level, as well as of all higher levels, get corrected. Moreover, the corrections contain contributions that produce a finite result if integrated over y, $I_n = \int dy\,\delta J_n(y) = I_1\sqrt{n}$, where $I_1 \equiv -\mathcal{J}\gamma_k/\omega_{\mathrm{Bk}}$. The results are shown in Fig. 4.

V. ANDREEV SPECTROSCOPY

The predicted spectral properties of the junction may be experimentally assessed via microwave spectroscopy techniques [25–29]. To drive the transitions between the Andreev levels [30], one subjects the system to an external time-dependent flux (now not only formally) which leads again to Eqs. (13) and (14).

It follows that to understand the transitions in our system we have to analyze the matrix elements of the current operator in Eq. (14) because it multiplies the externally applied time-dependent flux in Eq. (13). We thus evaluate $I_{n,n'} = \sum_k \int_0^L dy \langle\Psi_{n,k}(y)| j_k(y) |\Psi_{n',k}(y)\rangle$.
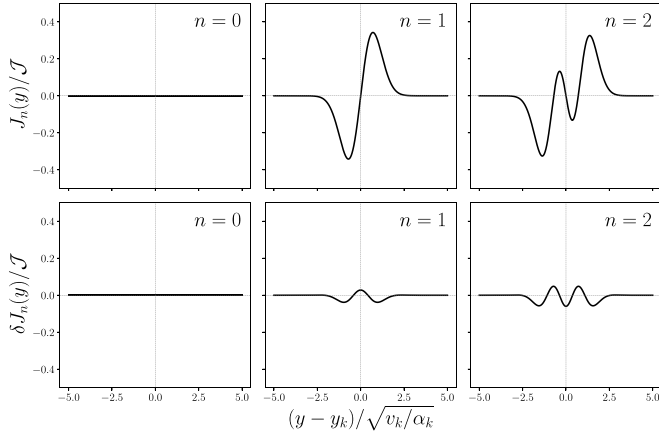
FIG. 4. Current profiles of the individual CdGM states. The upper panels correspond to the unperturbed states. The lower panels show the corrections (with $\gamma_k/\omega_{\mathrm{Bk}} = 0.05$) due to the gradient of the width $W(y)$.

Naturally, we find that $I_{n,n} = 0$, that is there is no net current without disorder, as discussed above. We find that the only nonzero matrix elements are

$$I_{n,n+1} = I_{n,-(n+1)} = -I_{n+1,-n} = -I_{-(n+1),-n} \approx \frac{1}{2}\tilde{I},$$

$$I_{0,1} = I_{0,-1} = -I_{-1,0} = -I_{1,0} \approx \frac{1}{i\sqrt{2}}\tilde{I}, \qquad (17)$$

where $\tilde{I} = \frac{\Delta}{1+W/\xi}\frac{\pi}{\Phi_0}$.

This analysis indicates that, at absolute zero, absorption transitions happen at frequencies $\Omega_{n,k} = \omega_{\mathrm{Bk}}(\sqrt{n} + \sqrt{n-1})$, $n = 1, 2, \ldots$, involving the pairwise population of neighboring CdGM levels with energies $\omega_{\mathrm{Bk}}\sqrt{n}$ and $\omega_{\mathrm{Bk}}\sqrt{n-1}$, by two quasiparticles (see Fig. 5). For $n = 1$ this transition requires flipping the parity of the Majorana zero energy state (more precisely of the fermion state formed by this zero-energy level and by another one, which could be at a different vortex or at the system's boundary).
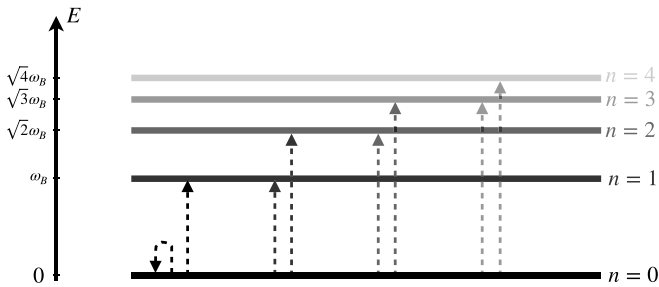

FIG. 5. The schematic depiction of the allowed transitions in vortex atoms. In particular, by driving the system at frequencies $\Omega = \omega_B(\sqrt{n} + \sqrt{n-1})$, $n = 1, 2, \ldots$ it is possible to break Cooper pairs in the ground state to populate pairs of neighboring excited states at energies $\omega_B\sqrt{n}$ and $\omega_B\sqrt{n-1}$.
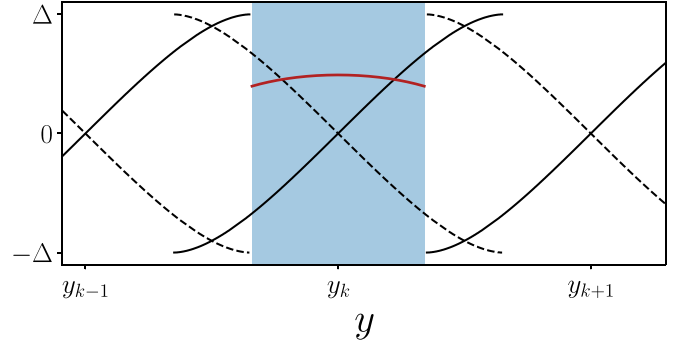

FIG. 6. The solid ($\sigma = +$) and the dashed ($\sigma = -$) black lines are the eigenenergies of the auxiliary Hamiltonian of Eq. (A1). The blue area indicates roughly the domain of one vortex. The red line shows a typical profile of the velocity $v_k(y)$.

VI. CONCLUSIONS AND OUTLOOK

In this paper, we present a study of the properties of Caroli-de Gennes-Matricon (CdGM) states associated with Josephson vortex atoms, where the CdGM states of different vortices remain nonoverlapping, in topological Josephson junctions. Our analysis provides insights into the recently observed nonzero critical currents in junctions hosting an integer number of vortices, linking this phenomenon to the response of low-lying CdGM states to perturbations that disrupt translational symmetry at the scale of a single magnetic length. We have investigated the current profiles of individual CdGM states under such perturbations and found that the current profiles of all states, except the zero-energy Majorana state, are modified, resulting in a finite total current. Additionally, we propose a method to probe the low-lying excitations of topological Josephson junctions through microwave spectroscopy, predicting a particularly clear pattern of resonances in the system.

Notice that, in this paper, we do not discuss the geometric (Shapiro-like) effects leading to the appearance of relatively large Josephson currents (at relatively high temperatures) in square-shaped Corbino junctions when the number of flux quanta is a multiple of four [11]. Here, we concentrate on a weaker geometric effect in strictly circular Corbino junctions, i.e., the irregularity of the junction's width. This leads to much smaller Josephson currents, which show up at very low temperatures at arbitrary numbers of flux quanta [11].

Several questions and intriguing directions were not addressed in the current research and should be explored in future studies. How do the results change beyond the atomic limit when there is an overlap between the CdGM states? What is the impact of Zeeman coupling, and what role do fluctuations in the phase of the order parameter play? Can these fluctuations mediate interactions between the CdGM states that are stronger than the exponentially small hybridization? We anticipate that in the long junction limit, it may be crucial to incorporate phase fluctuations in a self-consistent manner, considering the back-reaction of the current on the magnetic field. It would also be interesting to study the effect of the inhomogeneities of the chemical potential μ_N and of the induced gap Δ on the Josephson current.
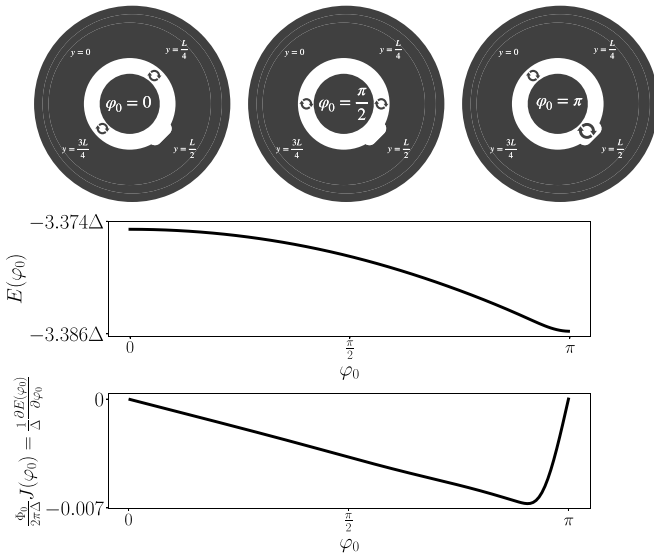
FIG. 7. This figure illustrates how the energy of Josephson vortices in a Corbino junction with a single extended impurity (widening) varies according to their position, set by the external phase difference φ_0. The upper panel is a cartoon of a Corbino junction with a single extended widening and two trapped vortices. The middle panel shows the contribution of the CdGM states to the ground-state energy $E(\varphi_0) = -\frac{1}{2}\sum_{n=1}^{n_{\max}} E_n(\varphi_0)$, while the lower panel shows the corresponding Josephson current $J(\varphi_0) = \frac{2\pi}{\Phi_0}\frac{\partial E(\varphi_0)}{\partial \varphi_0}$. As one would naively expect, a local increase in the junction width W locally increases the oscillator frequencies $\omega_{\mathrm{Bk}}/\Delta \sim \sqrt{W/\ell_B}$, reducing the total ground-state energy of the system. The simulations were performed in the regime $W \ll \xi$ with $L = 40W$ and a single widening located at $y = L/2$, spread over the length of $3L/10\pi$, and with $\delta W = W/10$. The order of magnitude of the Josephson current is consistent with the estimate (12).

In the last stages of preparation for this paper, a closely related paper was submitted [31]. In contrast with the study of Ref. [31] of open-ended geometry, here we discuss the Corbino geometry. We arrive at similar results for the microwave spectroscopy. The authors of Ref. [31] indicate that the lifting of the zeros in the Fraunhofer pattern may be related to the boundary conditions at the open ends. Our results in the current paper suggest that irregularities could also play a role in lifting these zeros.

ACKNOWLEDGMENTS

APPENDIX A: EFFECTIVE SINGLE-VORTEX HAMILTONIAN

To derive an effective Hamiltonian of a single vortex, we follow Ref. [16] and consider first the eigenstates of

$$h_0 = v\sigma_x\tau_z p_x - \mu(x)\tau_z + (\Delta(x,y)\tau_+ + \mathrm{H.c.}), \quad (A1)$$

treating the kinematics in y direction $h_1 = v\tau_z\sigma_y[p_y + eA_y(x)\tau_z]$ as a perturbation.

Assuming $W \ll \xi$, in the vicinity of $y \approx y_k = \ell_B/2 + k\ell_B$ (the blue region in Fig. 6), we approximate the wave function as a superposition of the $(\sigma = +)$ and $(\sigma = -)$ states

$$\Psi(x,y) \approx \sum_{\sigma=\pm} \alpha_{\sigma,k}(y)\psi_{\sigma,k}^{(0)}(x,y), \quad y \simeq y_k, \quad (A2)$$

where $\psi_{\sigma,k}^{(0)}(x,y)$ are the eigenfunctions of h_0 defined as

$$\psi_{\sigma,k}^{(0)}(x,y) = \sqrt{\frac{\kappa_k(y)}{2[1+\kappa_k(y)W]}} e^{i\frac{\pi y}{2\ell_B}\tau_z}\left[\Theta(-x)e^{i\sigma\mu_S x/v}e^{-i\sigma\mu_N W/2v}\begin{pmatrix} e^{-i\epsilon_k(y)W/2v} \\ \sigma e^{i\epsilon_k(y)W/2v} \end{pmatrix}e^{\kappa_k(y)x} \right.$$

$$+ \Theta(x)\Theta(W-x)e^{i\sigma\mu_N(x-W/2)/v}\begin{pmatrix} e^{i\epsilon_k(y)(x-W/2)/v} \\ \sigma e^{-i\epsilon_k(y)(x-W/2)/v} \end{pmatrix}$$

$$\left. + \Theta(x-W)e^{i\sigma\mu_S(x-W)/v}e^{i\sigma\mu_N W/2v}\begin{pmatrix} e^{i\epsilon_k(y)W/2v} \\ \sigma e^{-i\epsilon_k(y)W/2v} \end{pmatrix}e^{-\kappa_k(y)(x-W)}\right]|\sigma_x = \sigma\rangle, \quad (A3)$$

where $\sigma\varepsilon_k(y)$ is the corresponding eigenenergy shown in Fig. 6. The y dependent localization parameter κ_k, is defined through

$$v\kappa_k(y) = \sqrt{\Delta^2 - \varepsilon_k^2(y)} \equiv \Delta_k(y). \quad (A4)$$

Substituting the ansatz (A2) into the Schrödinger equation $(h_0 + h_1)\Psi = E\Psi$, we discover

$$\sum_{\sigma'=\pm}\left[v_k^{\sigma,\sigma'}(y)p_y\alpha_{\sigma',k}(y) + a_k^{\sigma,\sigma'}(y)\alpha_{\sigma',k}(y)\right] + \sigma\varepsilon_k(y)\alpha_{\sigma,k}(y) = E\alpha_{\sigma,k}(y), \quad (A5)$$
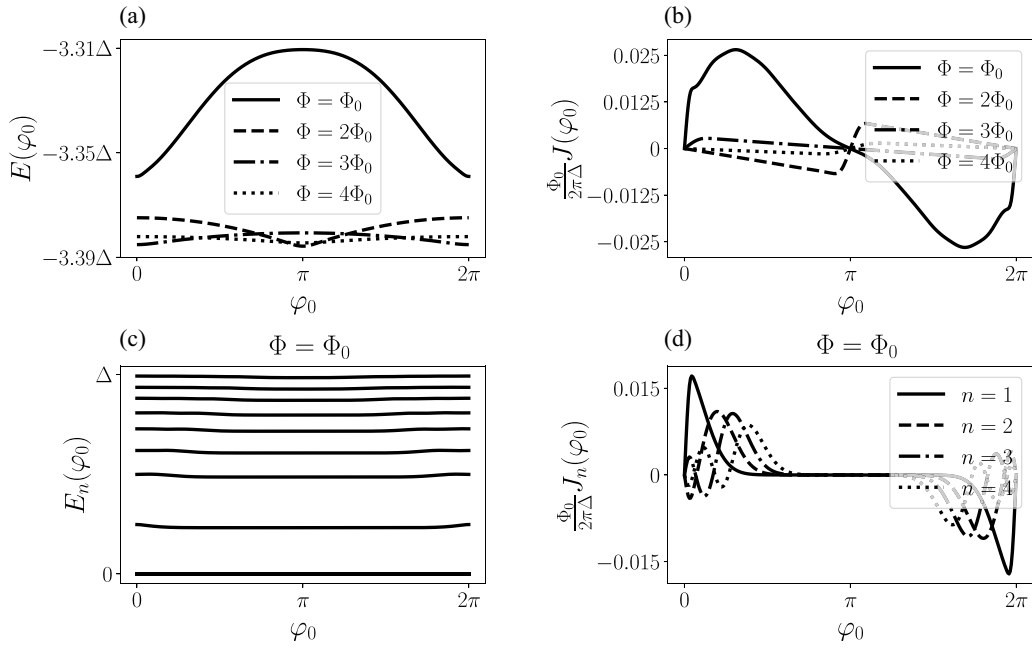
FIG. 8. Data for the Corbino junction with a single extended impurity (see Fig. 7). (a) The contribution of the CdGM states to the ground-state energy $E(\varphi_0) = -\frac{1}{2}\sum_{n=1}^{n_{max}} E_n(\varphi_0)$ for the total flux (fluxoid) $\Phi = N\Phi_0$, where $N = 1, 2, 3, 4$ is the number of trapped vortices. (b) The Josephson currents $J(\varphi_0) = \frac{2\pi}{\Phi_0}\partial_{\varphi_0} E(\varphi_0)$ corresponding to panel (a). (c) The phase-dispersion of the CdGM levels in a system with a single flux quantum. (d) Separate contributions of individual CdGM states to the current in the junction with a single flux quantum. The simulations were performed with the same parameters as in Fig. 7.

where

$$v_k^{\sigma,\sigma'}(y) = \int dx \psi_\sigma^\dagger(x, y - y_k) v \tau_z \sigma_y \psi_{\sigma'}(x, y - y_k)$$

$$= \frac{-i\sigma\delta_{\sigma',-\sigma} v}{1 + \frac{W(y)\tilde{\Delta}_k(y)}{v}} \left\{ \frac{\tilde{\Delta}_k(y)}{\mu_N} \sin\left(\frac{\mu_N W(y)}{v}\right) + \frac{\tilde{\Delta}_k(y)}{\mu_S^2 + \tilde{\Delta}_k^2(y)} \left[\tilde{\Delta}_k(y) \cos\left(\frac{\mu_N W(y)}{v}\right) - \mu_S \sin\left(\frac{\mu_N W(y)}{v}\right) \right] \right\}, \quad (A6)$$

$$a_k^{\sigma,\sigma'}(y) = \int dx \psi_\sigma^\dagger(x, y - y_k) h_1 \psi_{\sigma'}(x, y - y_k) = \frac{1}{2i} \frac{\partial v_k^{\sigma,\sigma'}(y)}{\partial y}. \quad (A7)$$

In this respect, the sought differential equation for the expansion coefficients $\alpha_{\sigma,k}$ becomes

$$\left(-\frac{1}{2}\{v_k(y), p_y\}\rho_y + \varepsilon_k(y)\rho_z \right) \begin{pmatrix} \alpha_{+,k}(y) \\ \alpha_{-,k}(y) \end{pmatrix} = E \begin{pmatrix} \alpha_{+,k}(y) \\ \alpha_{-,k}(y) \end{pmatrix}. \quad (A8)$$

APPENDIX B: EXAMPLE OF IRREGULARITY

In Figs. 7 and 8, we demonstrate a particular realization of an irregular $W(y)$.

APPENDIX C: CURRENT OPERATOR

We consider the projection of the current-density operator in the normal part of the system ($x \in [0, W]$) near $y \approx y_k$:

$$\frac{ve}{2}\Psi^\dagger(x, y)\sigma_x\Psi(x, y) \approx \frac{ve}{2}\sum_{\sigma=\pm} \sigma|\psi_{\sigma,k}(x, y)|^2 |\alpha_{\sigma,k}(y)|^2$$

$$= \frac{ve}{2}\frac{\kappa_k(y)}{1 + \kappa_k(y)W(y)}\sum_{\sigma=\pm}\sigma|\alpha_{\sigma,k}(y)|^2. \quad (C1)$$

Further one uses that

$$\frac{\partial\varepsilon_k(y)}{\partial y} = \frac{\pi}{\ell_B}\frac{v\kappa_k(y)}{1 + \kappa_k(y)W(y)}$$

to recover the result stated in the main text.

APPENDIX D: PERTURBATIVE EXPANSION

We treat the last term of (16) perturbatively, i.e., we split $h_k^{eff} = H_0 + V$, where $H_0 \equiv -i\bar{v}_k\rho_y\partial_y + \alpha_k(y - y_k)\rho_z$ and $V \equiv \frac{\gamma_k}{2}\{-i\partial_y, (y - y_k)\}\rho_y$.

A standard procedure,

$$y - y_k = \sqrt{\frac{\bar{v}_k}{2\alpha_k}}(a^\dagger + a), \quad -i\partial_y = i\sqrt{\frac{\alpha_k}{2\bar{v}_k}}(a^\dagger - a), \quad (D1)$$

leads to

$$H_0 = \frac{\omega_{Bk}}{2}[(a^\dagger + a)\rho_z + i(a^\dagger - a)\rho_y]. \quad (D2)$$

Here $\omega_{\mathrm{Bk}} \equiv \sqrt{2\alpha_k \bar{v}_k}$. For the perturbation we obtain

$$V = \frac{i\gamma_k}{2} \rho_y (a^{\dagger 2} - a^2). \tag{D3}$$

The eigenstates and the eigenvalues of H_0 are

$$|\Psi_0\rangle = i|0\rangle|\downarrow_x\rangle \quad \text{with} \quad E_0 = 0, \tag{D4}$$

(the factor i is needed to make this state invariant under charge conjugation $C = \rho_x K$) and

$$|\Psi_n\rangle = \frac{1}{\sqrt{2}}(|n-1\rangle|\uparrow_x\rangle + |n\rangle|\downarrow_x\rangle), \tag{D5}$$

$$|\Psi_{-n}\rangle = \frac{1}{\sqrt{2}}(|n-1\rangle|\uparrow_x\rangle - |n\rangle|\downarrow_x\rangle), \tag{D6}$$

with $E_{n,k} = -E_{-n,k} = \omega_{\mathrm{Bk}}\sqrt{n}$. Here $n > 0$. The states $|n\rangle \equiv \phi_n(y - y_k)$ are the standard eigenstates of a harmonic oscillator. As required $|\Psi_{-n}\rangle = C|\Psi_n\rangle$.

For the current profiles of the unperturbed states we obtain $J_0(y) = 0$ and

$$J_n(y) = \langle\Psi_n| j_k(y) |\Psi_n\rangle = \mathcal{J}\phi_{n-1}(y - y_k)\phi_n(y - y_k), \tag{D7}$$

where $\mathcal{J} \equiv \ell_B \alpha_k / \Phi_0$. All these profiles integrate to zero, as expected.

We perform the standard first-order perturbation expansion in γ_k and obtain the corrections $\delta J_n(y)$. The first two corrections read

$$\delta J_0(y) \equiv 0, \tag{D8}$$

$$\delta J_1(y) = -\frac{\mathcal{J}\gamma_k}{6\omega_{\mathrm{Bk}}}(6\phi_1^2 - \sqrt{6}\phi_1\phi_3 + 3\sqrt{2}\phi_0\phi_2 - 2\sqrt{6}\phi_0\phi_4). \tag{D9}$$

The arguments of the ϕ_n function on the RHS are all $y - y_k$.

---

[1] A. Y. Kitaev, Unpaired Majorana fermions in quantum wires, Phys. Usp. **44**, 131 (2001).

[2] Y. Oreg, G. Refael, and F. von Oppen, Helical liquids and Majorana bound states in quantum wires, Phys. Rev. Lett. **105**, 177002 (2010).

[3] R. M. Lutchyn, J. D. Sau, and S. Das Sarma, Majorana fermions and a topological phase transition in semiconductor-superconductor heterostructures, Phys. Rev. Lett. **105**, 077001 (2010).

[4] L. Fu and C. L. Kane, Superconducting proximity effect and Majorana fermions at the surface of a topological insulator, Phys. Rev. Lett. **100**, 096407 (2008).

[5] L. Fu and C. L. Kane, Josephson current and noise at a superconductor/quantum-spin-Hall-insulator/superconductor junction, Phys. Rev. B **79**, 161408(R) (2009).

[6] S. Nadj-Perge, I. K. Drozdov, B. A. Bernevig, and A. Yazdani, Proposal for realizing Majorana fermions in chains of magnetic atoms on a superconductor, Phys. Rev. B **88**, 020407(R) (2013).

[7] M. Aghaee *et al.* (Microsoft Quantum), InAs-Al hybrid devices passing the topological gap protocol, Phys. Rev. B **107**, 245423 (2023).

[8] G. Yue, C. Zhang, E. D. Huemiller, J. H. Montone, G. R. Arias, D. G. Wild, J. Y. Zhang, D. R. Hamilton, X. Yuan, X. Yao, D. Jain, J. Moon, M. Salehi, N. Koirala, S. Oh, and D. J. Van Harlingen, Signatures of Majorana bound states in the diffraction patterns of extended superconductor–topological insulator–superconductor Josephson junctions, Phys. Rev. B **109**, 094511 (2024).

[9] S. Nadj-Perge, I. K. Drozdov, J. Li, H. Chen, S. Jeon, J. Seo, A. H. MacDonald, B. A. Bernevig, and A. Yazdani, Observation of Majorana fermions in ferromagnetic atomic chains on a superconductor, Science **346**, 602 (2014).

[10] Y. Zhang, Z. Lyu, X. Wang, E. Zhuo, X. Sun, B. Li, J. Shen, G. Liu, F. Qu, and L. Lü, AC Josephson effect in Corbino-geometry Josephson junctions constructed on Bi$_2$Te$_3$ surface, Chin. Phys. B **31**, 107402 (2022).

[11] J. Y. Park, T. Werkmeister, J. Zauberman, O. Lesser, L. Anderson, Y. Ronen, S. Kushwaha, R. Cava, Y. Oreg, and P. Kim, Corbino Josephson interferometry on a surface of

topological insulator Sn-doped Bi$_{1.1}$Sb$_{0.9}$Te$_2$S, Bull. Am. Phys. Soc. (2024).

[12] C. Caroli, P. G. de Gennes, and J. Matricon, Bound fermion states on a vortex line in a type II superconductor, Phys. Lett. **9**, 307 (1964).

[13] E. Grosfeld and A. Stern, Observing Majorana bound states of Josephson vortices in topological superconductors, Proc. Natl. Acad. Sci. USA **108**, 11810 (2011).

[14] A. C. Potter and L. Fu, Anomalous supercurrent from Majorana states in topological insulator Josephson junctions, Phys. Rev. B **88**, 121109(R) (2013).

[15] S. S. Hegde, G. Yue, Y. Wang, E. Huemiller, D. Van Harlingen, and S. Vishveshwara, A topological Josephson junction platform for creating, manipulating, and braiding Majorana bound states, Ann. Phys. (NY) **423**, 168326 (2020).

[16] S. Backens, A. Shnirman, and Y. Makhlin, Topological Josephson junction in transverse magnetic field, JETP Lett. **116**, 891 (2022).

[17] M. Z. Hasan and C. L. Kane, *Colloquium*: Topological insulators, Rev. Mod. Phys. **82**, 3045 (2010).

[18] Unlike in Ref. [13] and similar to Refs. [14–16], we consider only the case when the phase grows linearly with y. Thus, we assume the regime $\lambda_J \gg \ell_B$, where λ_J is the Josephson penetration length [32]. This is justified if the effective Josephson energy of the junction is sufficiently small, or, alternatively, if the kinetic inductance of the superconducting films is sufficiently low.

[19] M. Titov and C. W. J. Beenakker, Josephson effect in ballistic graphene, Phys. Rev. B **74**, 041401(R) (2006).

[20] S. Backens and A. Shnirman, Current-phase relation in a topological Josephson junction: Andreev bands versus scattering states, Phys. Rev. B **103**, 115423 (2021).

[21] These are very important when the CdGM states of the vortices overlap.

[22] M. Hays, V. Fatemi, K. Serniak, D. Bouman, S. Diamond, G. de Lange, P. Krogstrup, J. Nygård, A. Geresdi, and M. H. Devoret, Continuous monitoring of a trapped superconducting spin, Nat. Phys. **16**, 1103 (2020).

[23] M. Hays, V. Fatemi, D. Bouman, J. Cerrillo, S. Diamond, K. Serniak, T. Connolly, P. Krogstrup, J. Nygård, A. L. Yeyati, A. Geresdi, and M. H. Devoret, Coherent manipulation of an Andreev spin qubit, Science **373**, 430 (2021).

[24] Y. Fauvel, J. S. Meyer, and M. Houzet, Opportunities for the direct manipulation of a phase-driven Andreev spin qubit, Phys. Rev. B **109**, 184515 (2024).

[25] L. Bretheau, Ç. Ö. Girit, C. Urbina, D. Esteve, and H. Pothier, Supercurrent spectroscopy of Andreev states, Phys. Rev. X **3**, 041034 (2013).

[26] L. Tosi, C. Metzger, M. F. Goffman, C. Urbina, H. Pothier, S. Park, A. L. Yeyati, J. Nygård, and P. Krogstrup, Spin-orbit splitting of Andreev states revealed by microwave spectroscopy, Phys. Rev. X **9**, 011010 (2019).

[27] P. D. Kurilovich, V. D. Kurilovich, V. Fatemi, M. H. Devoret, and L. I. Glazman, Microwave response of an Andreev bound state, Phys. Rev. B **104**, 174517 (2021).

[28] A. Bargerbos, M. Pita-Vidal, R. Žitko, L. J. Splitthoff, L. Grünhaupt, J. J. Wesdorp, Y. Liu, L. P. Kouwenhoven, R. Aguado, C. K. Andersen *et al.*, Spectroscopy of spin-split Andreev levels in a quantum dot with superconducting leads, Phys. Rev. Lett. **131**, 097001 (2023).

[29] J. J. Wesdorp, F. J. Matute-Cañadas, A. Vaartjes, L. Gruenhaupt, T. Laeven, S. Roelofs, L. J. Splitthoff, M. Pita-Vidal, A. Bargerbos, D. J. van Woerkom, P. Krogstrup, L. P. Kouwenhoven, C. K. Andersen, A. L. Yeyati, B. vanHeck, and G. deLange, Microwave spectroscopy of interacting Andreev spins, Phys. Rev. B **109**, 045302 (2024).

[30] An alternative to the flux (current) drive (see Refs. [22–24], for example) would be the gate drive as in Refs. [28,33].

[31] K. Laubscher and J. D. Sau, Detection of Majorana zero modes bound to Josephson vortices in planar S-TI-S junctions, arXiv:2411.00756.

[32] M. Tinkham, *Introduction to Superconductivity*, 2nd ed. (Dover Publications, 2004).

[33] C. Padurariu and Y. V. Nazarov, Theoretical proposal for superconducting spin qubits, Phys. Rev. B **81**, 144519 (2010).